Chemosphere 287 (2022) 132138

Contents lists available at ScienceDirect

Chemosphere

journal homepage: www.elsevier.com/locate/chemosphere

Examining samarium sorption in biochars and carbon-rich materials for water remediation: batch vs. continuous-flow methods

Joan Serra-Ventura, Miquel Vidal, Anna Rigol *

Department of Chemical Engineering and Analytical Chemistry, Faculty of Chemistry, University of Barcelona, Martí i Franquès 1-11, 08028, Barcelona, Spain

HIGHLIGHTS

- Batch and continuous-flow methods were valid to determine Sm sorption capacities.
- Cation exchange was a relevant mechanism for Sm sorption in biochars.
- Biochars and coal fines are green alternatives to activated charcoals for Sm sorption.

GRAPHICAL ABSTRACT

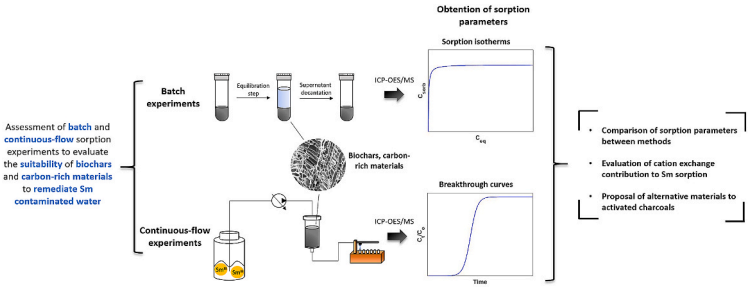

ARTICLE INFO

Handling Editor: Chang Min Park

Keywords:
Samarium
Biochars
Carbon-rich materials
Water remediation
Sorption methods
Sorption mechanisms

ABSTRACT

Samarium (Sm) sorption from aqueous solutions was evaluated in biochars (derived from castor meal (CM), eucalyptus forest residues (CE), sugarcane bagasse (SB) and green pericarp of coconut (PC)) and in other carbon-rich materials (coal fines (CF); two commercial activated charcoals (GAC, NGAC)) by applying batch and continuous-flow sorption experiments. Batch experiments revealed great K_d values, in the range of 10^4–10^5 L kg^{-1}, and high Sm sorption percentages (>97%, except for SB) in the range of environmental representative concentrations, using as-received materials, with no further treatments. Maximum sorption capacities were derived from sorption isotherms using the Langmuir model (from 1.2 to 37 mg g^{-1}). Continuous-flow sorption experiments permitted to obtain maximum sorption capacities by mass balance and by fitting the experimental breakthrough curves to Thomas and Yan models. CF exhibited the greatest maximum sorption capacity (40 mg g^{-1}) besting the commercial activated charcoals, while CM was established as the best biochar (7.2 mg g^{-1}), with similar results to NGAC (12 mg g^{-1}) but worse than GAC (36 mg g^{-1}). The contribution of cation exchange in Sm sorption was confirmed to be significant for most materials based on the analyses of cations leached during continuous-flow sorption experiments. Maximum sorption capacities derived from Langmuir fitting correlated well with maximum sorption capacities obtained from continuous-flow experiments. Both methods were confirmed to be suitable to determine the maximum Sm sorption capacity of the materials and then to propose the most suitable materials that can act as alternative to commercial activated charcoals.

* Corresponding author.
E-mail address: annarigol@ub.edu (A. Rigol).

https://doi.org/10.1016/j.chemosphere.2021.132138
Received 25 May 2021; Received in revised form 1 August 2021; Accepted 31 August 2021
Available online 2 September 2021

1. Introduction

Lanthanides (LN) are considered contaminants of emerging concern. They are present in fertilisers (Otero et al., 2005) and in industrial activities producing lightning devices and magnets, among others (Goonan, 2011). Recently, rising demand and difficulties associated with recycling (Jowitt et al., 2018) have led to an increase in LN environmental levels at worldwide scale. Amongst LN, La, Ce, Sm and Gd are the most relevant elements due to their large impact in soils, sediments, and water compartments. Currently, areas in central and south Africa and America are facing higher concentrations of LN in soils near industrial and mining areas than historical background records (Adeel et al., 2019). Clear signs of anthropogenic LN in water and soils have also been reported around Europe (Kulaksiz and Bau, 2013; Rogan et al., 2012; Möller et al., 2014). China, as world's first LN producer and supplier (Zhou et al., 2017) faces numerous cases of severe LN pollution (He et al., 2010; Jinxia et al., 2010; Mao et al., 2011). He et al. (2010) reported concentrations between 1 and 3 mg L^{-1} of various LN in effluents of Yellow River, several orders of magnitude higher than in non-contaminated sections of the same river, around 1–2 μg L^{-1}. This may lead to significantly higher concentrations in vegetables from mining areas than in controlled areas (2.49 and 1.23 μg kg^{-1} Sm, respectively), which is of concern in a long-term exposure (Zhuang et al., 2017).

Therefore, there is a rising interest to remediate LN affected areas, by either decreasing LN mobility in soils or removing LN from water bodies that can be used in soil irrigation or eventually incorporate into drinking water. Different physicochemical water treatments used for the removal of heavy metals could be appropriate for LN, although their efficiency has not yet been fully tested. Currently, treatments such as chemical precipitation and the use of ion-exchange resins are the most effective for effluents with inorganic cationic pollutants at a wide range of concentrations due to their operational simplicity and high removal efficiency (Kurniawan et al., 2006; Fu and Wang, 2011). The use of sorbents for water remediation is also gaining attention. Besides the widespread use of activated charcoal (Smith et al., 2016; Iannicelli-Zubiani et al., 2018), new materials such as biochar arise as an alternative of increasing interest. Biochar is obtained from the pyrolysis of forestry, agricultural or municipal biomass in an oxygen-reduced atmosphere. Hence, the use of biochar implies a sustainable exploitation of terrestrial resources, with an associated lowered environmental impact, promoting a circular economy in the wastewater treatment (Ahmad et al., 2014; IBI, 2018). Moreover, the use of lower pyrolysis temperatures (e.g. slow pyrolysis at 350 °C in front of 800–1000 °C in activated charcoals) and the absence of a physical or chemical activation step results in an improved cost effectiveness, compared to the obtention of activated charcoals (Manyà, 2019; Tagliaferro et al., 2020). Feedstock origin and pyrolysis temperature of biomass, among other factors, affect the physicochemical properties of the resulting biochar, such as specific surface area and micro porosity, and thus its sorption capacity (Ronsse et al., 2013; Ding et al., 2014; Tan et al., 2015). Whereas sorption mechanisms for heavy metals have been proposed, such as cation exchange and complexation (Li et al., 2017; Mahdi et al., 2018), additional mechanisms for LN sorption in biochar, such as electrostatic interaction, have also been suggested from the presence of functional groups in infrared spectra of the biochar (Torab-Mostaedi et al., 2015).

Laboratory experiments are required to assess the efficiency of target sorbents before its application at field scale in the management of contaminated waters and soils. Thus, the present work focuses on the assessment of batch and continuous-flow sorption methods to evaluate the sorption and removal of LN from aqueous solutions by biochar and other carbon-rich materials, such as coal fines and activated charcoals, as received with no further treatments. Batch sorption experiments allow to quantify the dependence of sorption capacity with the initial concentration, to obtain information about the distribution between the LN and the target material at concentrations of environmental concern, and to predict the maximum efficiency of the material to reduce LN concentration in contaminated waters. On the other hand, as water remediation may be based on a filtering process where biochar would act as a biofilter (Boehm et al., 2020), continuous-flow sorption experiments are better option to examine the dynamics of the sorption process, also permitting to estimate the maximum sorption capacity of biochar when treating contaminated waters. To date, fewer results have been reported with regards to Sm removal using continuous-flow conditions than using batch tests (Hadjittofi et al., 2016), and it has not yet been examined whether both approaches may lead to similar results. In this work, Sm is selected as representative for LN. After performing the experiments, sorption isotherms from batch experiments and continuous-flow breakthrough curves are fitted to mathematical models with the aim to predict the sorption patterns and compare derived parameters of the tested materials. Finally, a proposal is made of the most suitable materials for the treatment of LN contaminated waters.

2. Materials and methods

2.1. Materials

Four biochars produced by slow pyrolysis at a temperature of 350 °C, heating rate of 5 °C min^{-1}, and residence time of 70 min (Doumer et al., 2015) were used in this work. Their feedstocks were: castor meal (CM), eucalyptus forest residues (CE), sugarcane bagasse (SB), and green pericarp of coconut (PC). Biochars were sieved to a particle size <2 mm before analyses. More information about the materials is given in Section 1 of Supplementary Material.

Additionally, three carbon-rich materials were used to compare their Sm sorption capacity with that of biochars: coal fines (CF), and two commercial activated charcoals supplied by Merck: an untreated activated charcoal (GAC) and the steam-activated charcoal Norit® for potable water processing (NGAC). CF was sieved to <2 mm before analyses, whereas GAC and NGAC were analysed as received (GAC <2 mm; NGAC <1 mm).

The material's characterisation consisted in the analysis of total carbon, hydrogen, and oxygen (%C, %H, %O); total organic carbon (TOC), cation exchange capacity (CEC), pH at the point of zero charge (pH_{pzc}), specific surface area (SSA) at a particle size <2 mm and functional groups identification by Fourier-transform infrared spectroscopy (FT-IR) of materials before and after batch sorption experiments. More details about the physicochemical characterisation of materials is given in Section 2 of Supplementary Material.

2.2. Batch sorption experiments

2.2.1. Sorption isotherms

Stock Sm solutions were prepared by dissolving weighed amounts of $Sm(NO_3)_3{\cdot}6H_2O$ (Merck). Batch sorption experiments were performed in 80 mL polypropylene tubes. Two-gram samples of the materials were end-over-end shaken for 24 h (a suitable contact time to reach equilibrium (Frišták et al., 2017), as 6–8 h have been reported as enough to complete the sorption process (Kütahyali et al., 2010; Kołodyńska et al., 2018)) with 50 mL of Sm stock solutions, at initial concentrations within 0.06–10 meq L^{-1} range for biochars and 0.06–50 meq L^{-1} range for the rest of carbon-rich materials. Suspensions were centrifuged at 10,000 rpm for 15 min with a Beckman J2-HS Centrifuge. The resulting supernatants were decanted off and filtered through 0.45 μm nylon filters. Filtered supernatants were acidified to 1% HNO_3 and stored at 4 °C until analysis of Sm and major cations (Ca, Mg, K, Na).

Blank experiments were also performed equilibrating materials with double deionised water. Resulting supernatants were characterised in terms of dissolved organic carbon (DOC), pH, and water-soluble Sm, Ca, Mg, K, and Na.

The Sm sorbed concentration (C_{sorb}, mg kg^{-1}) was calculated from the initial (C_i, mg L^{-1}) and equilibrium (C_{eq}, mg L^{-1}) solution

concentrations using Eq. (1):

$$C_{sorb} = (C_i - C_{eq}) \cdot V/m \quad (1)$$

where m is the mass of material (kg) and V is the volume of solution added (L).

The solid-liquid distribution coefficient, K_d (L kg^{-1}), was calculated as the ratio between C_{sorb} and C_{eq} (Eq. (2)):

$$K_d = C_{sorb}/C_{eq} \quad (2)$$

In addition, sorption percentages (S, %) were calculated as follows:

$$S = (C_i - C_{eq})/C_i \cdot 100 \quad (3)$$

2.2.2. Fitting of sorption isotherms

The experimental values of C_{eq} and C_{sorb} obtained at increasing initial Sm concentrations were used to construct the sorption isotherms, which were subsequently fitted to the Langmuir model (Eq. (4)):

$$C_{sorb} = b \cdot K_L \cdot C_{eq}/(1 + K_L \cdot C_{eq}) \quad (4)$$

where b (mg kg^{-1}) estimates the maximum sorption capacity, which is related to the amount of available sorption sites of a given material, and K_L (L mg^{-1}), the Langmuir constant, represents the bonding energy of the available sites and it is related to the slope of the initial linear part of a Langmuir sorption isotherm. More information about the data treatment is given in Section 3 Supplementary Material.

2.2.3. Desorption test to evaluate sorption reversibility

The desorption tests were performed under the same conditions as sorption experiments, at three concentration levels (0.06, 1, and 6 meq L^{-1}). The remaining mass of material after the sorption experiments was dried prior to the desorption tests. Considering the supernatant concentration after the desorption test ($C_{eq,des}$, mg L^{-1}), the desorption percentages (D, %) were calculated as follows:

$$D = C_{eq,des} \cdot V \,/\, \left((C_i - C_{eq}) \cdot V + C_{eq} \cdot V_{rem}\right) \cdot 100 \quad (5)$$

where V_{rem} (L) is the remaining volume of solution after the sorption experiments.

2.3. Continuous-flow sorption experiments

2.3.1. Obtention of breakthrough curves

The set-up consisted in a column (1.6 cm internal diameter, 10 cm length) packed with 3–3.5 g of material, with silica filters on column top and bottom. The solutions were dispensed by a peristaltic pump (GILSON Minipuls 3) connected to the column. The packed material was first preconditioned with double deionized water for 20 min. Then, Sm solutions were pumped and effluent fractions were automatically collected with a fraction collector (GILSON FC 204) at specified time intervals, every 10 min from the start of the experiment up to 180 min and every 40 min from 180 min until the end of the experiment. A detailed scheme is presented in Fig. S1 in Supplementary Material. The total operation time (1200–2000 min) was adapted according to the sorption capacity that materials exhibited in previous batch assays. Collected fractions were acidified with a 1% HNO_3 concentration and stored at 4 °C until analysis.

To check whether initial conditions of flow rate and Sm concentration affect the assessment of the maximum sorption capacities of the materials, previous experiments with selected materials (PC and CF) were carried out. When testing flow rate, the experimental conditions were 0.25, 0.5, and 1 mL min^{-1}, at a Sm initial concentration of 5 meq L^{-1}. When testing the effect of initial Sm concentration, experimental conditions were 1, 2 and 5 meq L^{-1} for PC, and 5, 7.5 and 10 meq L^{-1} for CF, at a flow rate of 0.5 mL min^{-1} for the two materials.

To obtain the maximum sorption capacities of the materials within a reasonable operational time, the following conditions were used according to the sorption capacities obtained from the above-mentioned batch experiments: SB was assayed at 2 meq L^{-1} and 0.25 mL min^{-1}; CM, CE, PC at 5 meq L^{-1} and 0.25 mL min^{-1}; and CF, GAC, NGAC at 10 meq L^{-1} and 0.5 mL min^{-1}.

The breakthrough curves were obtained by plotting the ratio between Sm concentration at time t and the initial Sm concentration (C_t/C_o) versus time. More information about the possible different profiles of the breakthrough curves is given in Fig. S2 in Supplementary Material.

The sorbed Sm concentration (q_{exp}, mg g^{-1}) at time t was obtained by mass balance, following Eq. (6):

$$q_{exp} = m_{Sm} \Big/ m = \left(m_{in,t} - \sum_{i=to}^{t} m_{out,i}\right) \Big/ m = \left((C_o \cdot F \cdot t) - \sum_{i=to}^{t} (C_{t,i} \cdot F \cdot f)\right) \Big/ m \quad (6)$$

where m_{Sm} (mg) is the mass of Sm sorbed at time t obtained from the calculation of the Sm mass input ($m_{in,t}$) and output ($m_{out,i}$); F (L min^{-1}) is the flow rate; and f (min) is the elapsed time with which the fraction was collected. If the time corresponds to the total operation time, the maximum sorption capacity ($q_{exp,max}$) is obtained.

2.3.2. Elucidating the contribution of the cation exchange to Sm sorption

To assess the contribution of the cation exchange mechanism to Sm sorption, blank experiments with the materials were conducted to quantify the washed-off fraction of major cations (Ca, Mg, K, Na) in the absence of Sm. The blank assays were performed with the same experimental conditions of material mass, flow rate and operational time as those with Sm.

2.3.3. Fitting of breakthrough curves

The breakthrough curves were fitted to Thomas and Yan models to derive sorption parameters that do not depend on the operational time, unlike the previous q_{exp} quantified by mass balance.

The Thomas model integrates a pseudo-second order reversible kinetics and the sorption Langmuir equation. It assumes negligible axial and radial dispersion in the column and considers an extremely small external and internal diffusion resistances during the sorption process (Thomas, 1948). The model is described by the following non-linear equation (Eq. (7)):

$$C_t / C_o = 1 / (1 + \exp(K_{Th} \cdot (q_{Th} \cdot m - C_o \cdot F \cdot t) / F)) \quad (7)$$

where C_o (mg L^{-1}) is the initial concentration, C_t (mg L^{-1}) the concentration at time t (min), K_{Th} (L min^{-1} mg^{-1}) the Thomas rate constant, and q_{Th} (mg g^{-1}) the maximum sorption capacity predicted by the model. A limitation of this model is that when the experimental time is zero, the modelled C_t/C_o differs from zero, which is not consistent and can lead to predicted maximum sorption capacities deviated from those achieved experimentally (Yan et al., 2001; Xu et al., 2013).

The Yan model has recently been used to describe the sorption of cationic species in continuous-flow experiments (Araneda et al., 2011). It is an empirical model aiming at correcting the Thomas model deviations at short and long times of the breakthrough curve (Yan et al., 2001) due to a C_t/C_o value which is zero at zero time and an exponential factor adjusting the slope of the curve. It is represented by Eq. (8):

$$C_t/C_o = 1 - 1/(1 + (C_o \cdot F \cdot t/(q_{Yan} \cdot m))^a) \quad (8)$$

where q_{Yan} (mg g^{-1}) is the maximum sorption capacity predicted by the model and a is the dimensionless model parameter.

2.4. Analytical measurements

Sm and major cations (Ca, Mg, K, Na) present in the solutions originated from batch and continuous-flow sorption experiments were determined by inductively coupled plasma optical emission

spectroscopy (ICP-OES) and inductively coupled plasma mass spectrometry (ICP-MS). More details are given in Section 4 of the Supplementary Material.

3. Results and discussion

3.1. Physicochemical characterisation of materials

Main physicochemical properties of the samples were analysed to better discuss Sm sorption mechanisms. Table 1 summarises the main physicochemical properties of the tested materials. The C content increased from CF to biochars and activated charcoals, and derived C/H and C/O ratios were also much higher for activated charcoals due to their low O content. The C/O ratios are related to aromaticity (Suliman et al., 2016) and could affect the sorption capacity. Similar C and TOC values indicated no presence of carbonate phases. Activated charcoals presented the highest SSA, while CF and biochars exhibited much lower values denoting that it might not be the main factor affecting sorption. CEC values were high for all materials, with remarkably high values for CF and GAC, whereas SB and NGAC showed the lowest CEC values among the tested materials. The sum of the exchangeable cations and ΣM_{exch}/CEC ratios indicated a varying relative CEC occupancy among materials, with PC and GAC exhibiting the highest ratios. pH values ranged from slightly acid (SB) to basic (GAC). For biochars and CF, pH was higher than pH_{pzc}, thus indicating that surfaces were negatively charged due to the ionisation of oxygen-containing functional groups (i.e., carbonyl, carboxylic). Then, materials could establish electrostatic interactions with cations (Qiu et al., 2008). Biochars, especially CM and CE, exhibited the highest DOC values, whereas the lowest were observed for CF and activated charcoals. For all materials, the DOC concentrations were high enough to be able to chelate LN in solution (Xu et al., 2007; Armstrong and Wood, 2012). Finally, water-soluble concentrations of major cations were significant for all materials, with PC and CM showing the highest concentrations, and NGAC having the lowest concentration.

Considering the speciation of Sm at the sorption pH of the different materials, it can be anticipated that precipitation of $Sm(OH)_{3\,(s)}$ will not take part as a sorption mechanism. Thus, the Sm species that are expected to interact with the materials must be Sm^{3+} and $SmOH^{2+}$.

Table 1
Physicochemical properties of the materials.

Parameter	CM	CE	PC	SB	CF	GAC	NGAC
C (%)	55	70	65	65	50	75	79
H (%)	6	4	4	4	2	0.5	0.5
O (%)	22	26	24	22	21	9	2
C/H ratio	0.77	1.5	1.4	1.4	2.1	13	13
C/O ratio	3.3	3.6	3.6	3.9	3.2	11	53
TOC (%)	55	65	63	60	43	73	79
DOC (mg L^{-1})	1140	208	94	95	6.9	3.5	3.1
pH	7.3	7.2	7.2	6.0	8.0	10.1	8.7
pH_{pzc}	6.4	6.3	5.7	5.2	7.5	10.4	10.9
SSA (m^2 g^{-1})	<1	<1	<1	1.3	7.3	580	964
CEC (meq kg^{-1})	101	96	100	52	633	167	45
ΣM_{exch} (meq kg^{-1})	59	53	67	19	307	102	3.5
ΣM_{exch}/CEC ratio	0.58	0.55	0.67	0.36	0.48	0.61	0.08
Ca_{exch} (meq kg^{-1})	31	27	6.1	10	218	71	2.3
Mg_{exch} (meq kg^{-1})	17	13	9.3	2.9	59	26	0.38
K_{exch} (meq kg^{-1})	10	9.7	37	5.6	29	3.4	0.15
Na_{exch} (meq kg^{-1})	0.85	2.9	15	0.74	0.96	1.8	0.67
ΣM_{ws} (meq L^{-1})	8.1	3.5	16	1.5	2.8	3.5	0.26
Ca_{ws} (meq L^{-1})	1.4	0.63	0.042	0.45	0.33	0.40	0.13
Mg_{ws} (meq L^{-1})	2.0	1.1	0.24	0.32	0.28	1.1	0.025
K_{ws} (meq L^{-1})	4.7	1.3	10	0.70	2.1	1.5	0.063
Na_{ws} (meq L^{-1})	0.043	0.46	5.3	0.058	0.068	0.54	0.037

ΣM_{exch}: $Ca_{exch}+Mg_{exch}+K_{exch}+Na_{exch}$; WS: water soluble;
ΣM_{ws}: $Ca_{ws}+Mg_{ws}+K_{ws}+Na_{ws}$.

3.2. Examination of Sm sorption with batch tests

A similar Sm sorption pattern was observed for all materials. A C_{sorb} vs. C_{eq} Langmuir-shaped sorption isotherm was obtained, which consisted in an increase of C_{sorb} with C_i, until reaching a plateau at high concentrations, indicating the saturation of the sites involved in the Sm sorption and the absence of an on-going precipitation process. Fig. 1 plots the C_{sorb} vs. C_{eq} and K_d vs. C_{sorb} sorption isotherms obtained for CM, CF and the activated charcoal GAC. The sorption isotherms of the rest of the materials can be found in Fig. S3 in Supplementary Material.

High initial Sm concentrations were needed to saturate the CF and activated charcoals to evidence the Langmuir sorption pattern. The K_d vs. C_{sorb} representation showed that K_d values at the lowest C_i range were lower than expected, which can be attributed to competitive effects for Sm sorption due to the solution components. At this range, C_{eq} were around 10^{-3} meq L^{-1} for biochars, and 10^{-4}-10^{-5} meq L^{-1} for CF and activated charcoals, then enabling the formation of soluble chelates with DOC. Furthermore, competitive effects could also appear due to a much higher concentration of cations than Sm in solution, especially for CM and PC materials. Then, K_d increased with the increase in C_i, overcoming competitive effects and, subsequently, it decreased with a further C_i increase as sorption sites were saturated. In agreement with the conclusion from speciation studies, precipitation was discarded as sorption isotherms did not show the characteristic pattern for a precipitation phenomenon: a sharp increase in C_{sorb} at a reasonably constant value of C_{eq}.

Table 2 summarizes the sorption parameters derived from experimental data and Langmuir fitting. Maximum K_d values ($K_{d,max}$) higher than 10^5 L kg^{-1} were obtained for the activated charcoals, which are commercial materials prepared for having high sorption characteristics. Values of $K_{d,max}$ for biochars and CF were higher than 10^4 L kg^{-1} (except for the SB biochar, probably due to its lowest CEC among biochars and slightly acidic pH). With such high $K_{d,max}$ values, S_{max} were higher than 99.5% in all cases. Values of K_d at the lowest initial concentration ($K_{d,conc\ min}$) followed a similar sequence among materials to that of $K_{d,max}$. The lower values of $K_{d,conc\ min}$ than $K_{d,max}$, as mentioned before, were attributed to competition effects. Despite the presence of competitive effects at low C_i (more representative of the environmental concentration range), most biochars (except for SB) could remove more than 97% of Sm from the aqueous solution.

The maximum sorption capacity, derived from the b parameter of the Langmuir model, followed the CEC sequence, except for the NGAC material, for which can be anticipated that cation exchange would not be a relevant mechanism for Sm sorption. The rest of materials presented a good correlation between b and CEC (log-transformed data; $R^2 = 0.87$, p-value < 0.05), with a slope that did not statistically differ from one, suggesting that cationic exchange could be a relevant mechanism for Sm sorption, especially in biochars.

The lack of sorption data in the literature, in addition to the scarce characterisation of materials, hampers the comparison of our results with other studies, which often present treated materials with enhanced sorption capacities (Hadjittofi et al., 2016; Liatsou et al., 2017). The only possible comparison is with Frišták et al. (2017), who reported an europium (Eu) sorption capacity of 0.89 mg g^{-1}, much lower than the ones obtained in this work, in an untreated biochar with similar particle size to those of our materials.

Regarding desorption data, the low desorption percentages obtained (from 0.1 to 5.5% in biochars and coal fines, being completely negligible for the activated charcoals) revealed the high irreversibility of the Sm sorption process in the materials. Detailed information is given in Table S1 in Supplementary Material.

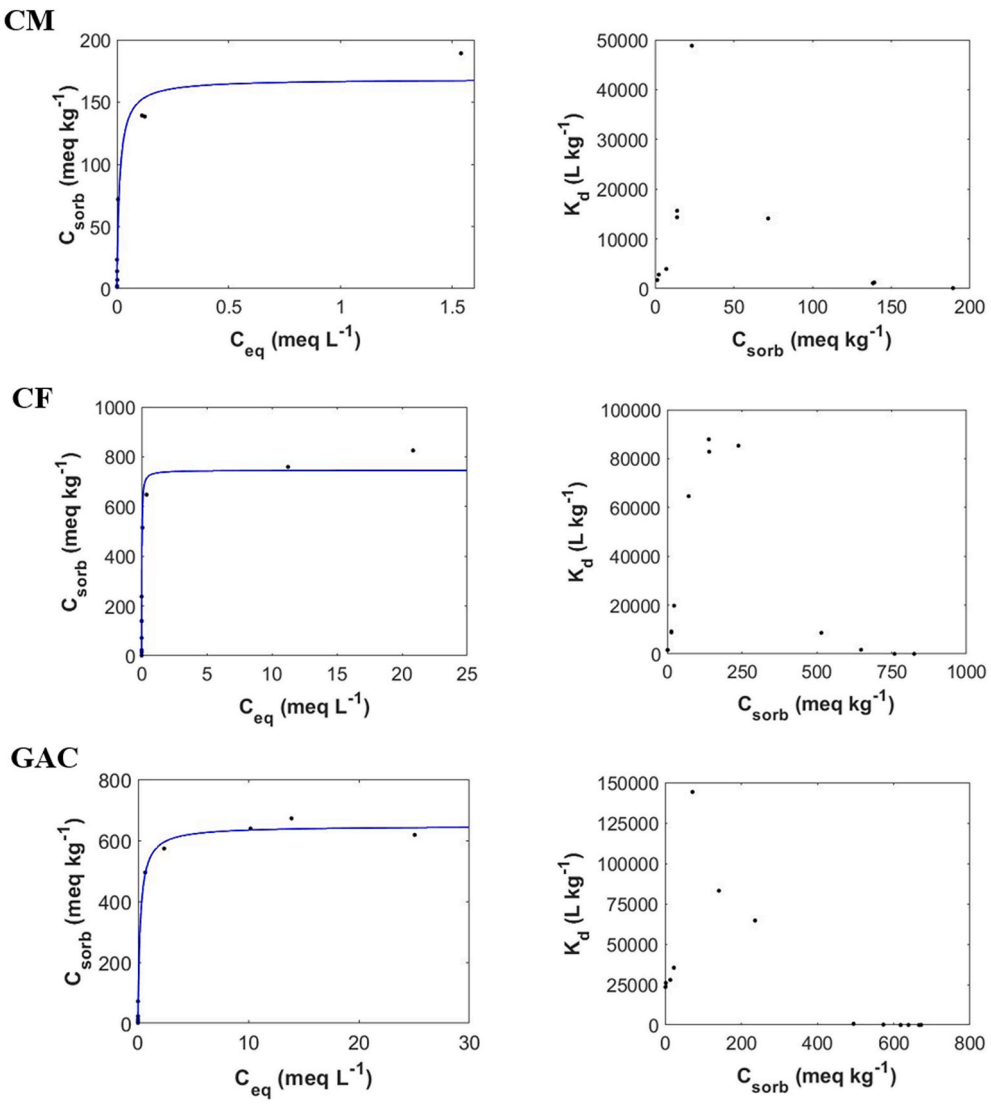

Fig. 1. C_{sorb} vs. C_{eq} sorption isotherms of CM, CF and GAC (left) fitted to Langmuir model (blue line) and K_d vs. C_{sorb} sorption isotherms of CM, CF and GAC (right). (For interpretation of the references to colour in this figure legend, the reader is referred to the Web version of this article.)

Table 2
Sorption parameters for the tested materials.

Material	$K_{d,conc\ min}$ (L kg^{-1})	$S_{conc\ min}$ (%)	$K_{d,max}$ (L kg^{-1})	S_{max} (%)	b (meq kg^{-1})
CM	1750	98.6	48800	99.9	169
CE	1350	98.2	14900	99.8	89
PC	859	97.2	75300	>99.9	127
SB	134	84.3	5110	99.5	23
CF	1570	98.4	87900	>99.9	746
GAC	23500	99.9	$>10^5$	>99.9	647
NGAC	12600	99.8	$>10^5$	>99.9	283

3.3. Examination of Sm sorption by continuous-flow experiments

3.3.1. Description and fitting of breakthrough curves

In a first step, PC and CF materials were used to check whether the flow rate and initial Sm concentration affected the final value of q_{exp}. Fig. S4 in the Supplementary Material plots the breakthrough curves and summarises the $q_{exp,max}$ obtained when varying these conditions. The first plateau was always observed for CF, whereas it was not for PC. The resulting $q_{exp,max}$ values depended much more on the material than on the experimental conditions. An increase in F, keeping C_o constant, did not lead to systematically higher $q_{exp,max}$ values, which kept relative constant for a given material. Regarding the effect of C_o, significant changes on the $q_{exp,max}$ were not either observed. Then, it was concluded that the maximum sorption capacity of PC and CF was not affected by F or C_o in the range of values tested. These conclusions were extrapolated to all the materials to be tested in this work.

Fig. 2 plots the breakthrough curves obtained for all the materials examined, along with their fittings to Thomas and Yan models. Biochars and activated charcoals revealed similar sorption profiles that were distant from the ideal breakthrough curves assumed by the fitting models, as the first plateau was not generally observed and significant site saturation was noted at short times. A progressive saturation from $C_t/C_o = 0.5$ onwards took place, although a complete saturation ($C_t/C_o = 1$) was not noticed. Unlike the rest of materials, CF nearly exhibited the ideal profile of a continuous-flow breakthrough curve, with a clear sigmoidal-shaped curve.

Table 3 summarises the values of $q_{exp,max}$ as well as of the sorption parameters derived from the fitting of the breakthrough curves to Thomas and Yan models. The highest $q_{exp,max}$ was exhibited by CF, even higher than that of activated charcoals, whereas CM presented the highest among biochars, in agreement with previous results from batch experiments.

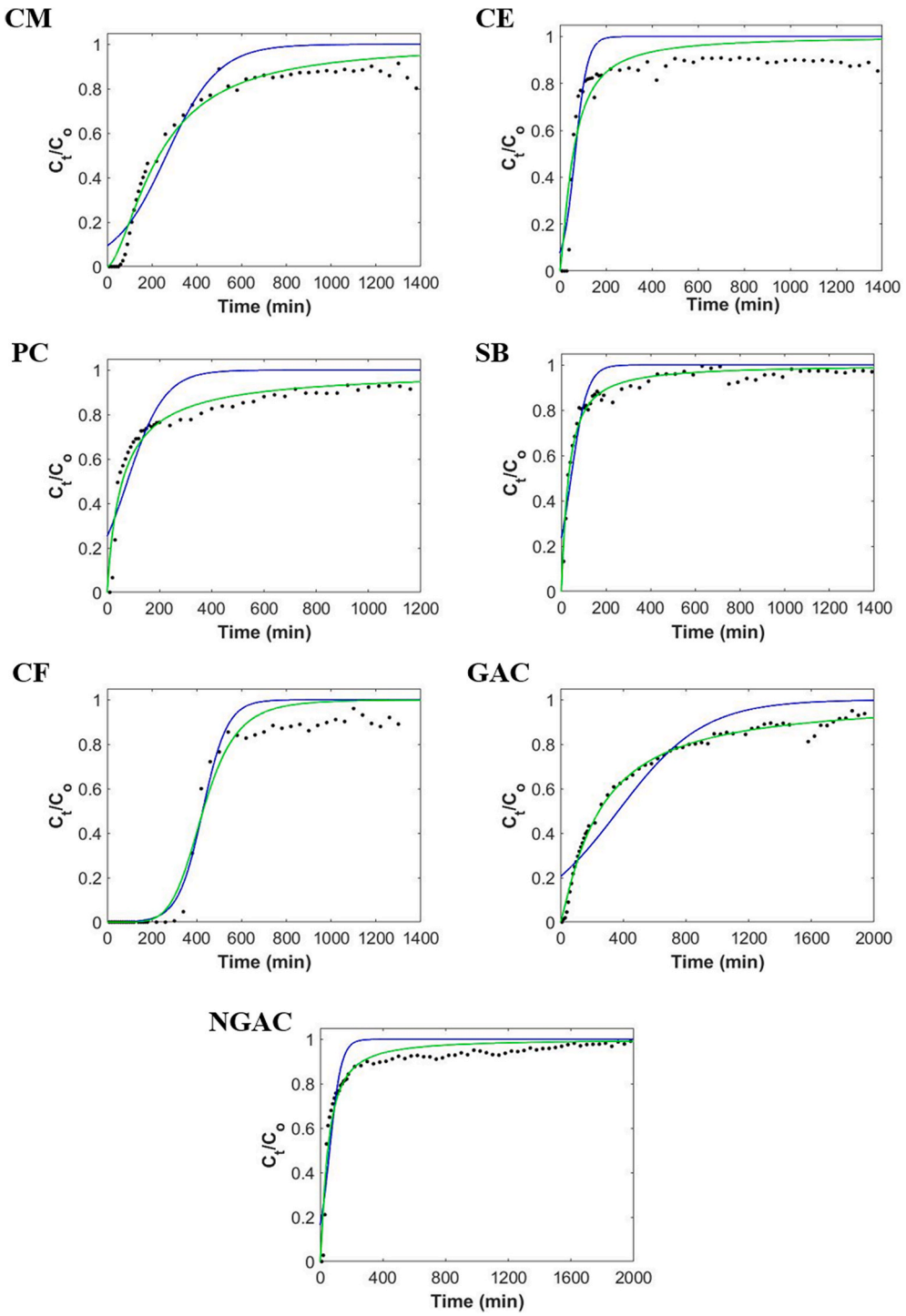

Fig. 2. Breakthrough curves of tested materials fitted to Thomas model (blue line) and Yan model (green line). (For interpretation of the references to colour in this figure legend, the reader is referred to the Web version of this article.)

Assuming the non-ideal pattern of the breakthrough curves for most materials in this work, it is expected that both models might show limitations in the fitting of the experimental data and subsequent prediction of sorption parameters. Yan model adjusted the data slightly better than Thomas model, with correlation coefficients generally higher than 0.95, probably due to the above-mentioned Thomas model limitations. Yan model adapts better to a wide range of sorption patterns due to the "a" parameter. Despite the limitations of the Thomas model fitting, the derived K_{Th} parameter was useful to quantitatively estimate the sorption rate towards a final state of saturation of the material. Higher K_{Th} indicated materials which were quickly saturated, such as CE and SB, whereas the opposite (slow saturation rate) was observed for other materials, such as GAC.

Differences between $q_{exp,max}$ and sorption capacities predicted by Thomas and Yan models were observed for a few materials, although the sequence of values among materials agreed. The models generally underestimated the maximum sorption capacity, probably caused by the general absence of ideal sigmoidal-shaped curves. In fact, the models best predicted the maximum sorption capacity for CF, which better adapted to an ideal breakthrough curve.

Table 3
Sorption parameters derived from the continuous-flow experiments for the tested materials.

Material	$q_{exp,max}$ (mg g^{-1})	Thomas model			Yan model		
		K_{Th} (L min^{-1} g^{-1})	q_{Th} (mg g^{-1})	R^2	a	q_{Yan} (mg g^{-1})	R^2
CM	7.2	0.032	5.2	0.90	1.6	4.6	0.98
CE	4.1	0.14	1.3	0.77	1.4	1.2	0.86
PC	3.8	0.051	1.6	0.71	0.96	1.2	0.95
SB	0.95	0.26	0.37	0.86	1.2	0.27	0.98
CF	40	0.032	36	0.97	5.7	36	0.97
GAC	36	0.0070	25	0.89	1.2	17	0.99
NGAC	12	0.051	4.3	0.85	1.3	3.4	0.95

3.4. Assessment of cationic exchange contribution to Sm sorption

The overall concentration of Ca+Mg+K+Na cations was quantified in the solutions originated from the continuous-flow experiments with Sm to assess the contribution of the cationic exchange mechanism to the sorption process. The overall concentration of Ca+Mg+K+Na had two contributions: cations solubilised (washed-off) by water (which are quantified with blank experiments) and cations exchanged with Sm. Therefore, the amount of sorbed Sm (expressed as meq L^{-1}) along the experiment can be compared with the Ca+Mg+K+Na concentrations attributed to an exchange process, obtained from the overall concentration minus the washed-off contribution. Details on the comparison between the Sm sorbed and Ca+Mg+K+Na exchanged profiles for all materials are given in Fig. S5 in Supplementary Material.

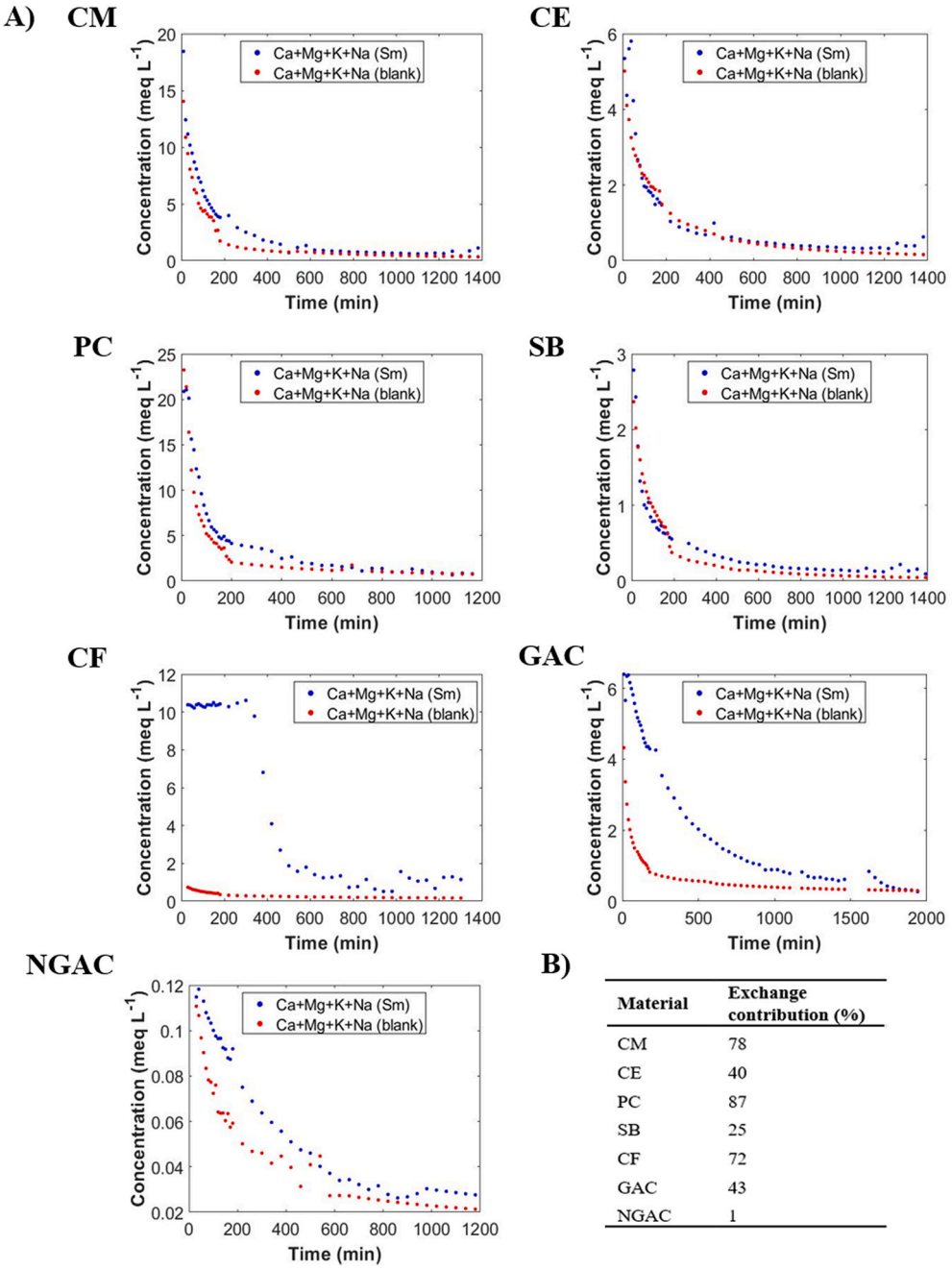

B)

Material	Exchange contribution (%)
CM	78
CE	40
PC	87
SB	25
CF	72
GAC	43
NGAC	1

Fig. 3. A) Changes over time of Ca+Mg+K+Na concentrations in collected fractions in experiments with Sm and without Sm (blank experiments) and B) Mean values of the cationic exchange contribution (%) to Sm sorption.

Fig. 3A plots the changes over time of the overall Ca+Mg+K+Na and washed-off concentrations, whereas Fig. 3B shows the ratio between the exchanged Ca+Mg+K+Na with respect to the sorbed Sm, as a way to estimate the cationic exchange contribution to Sm sorption. As these ratios slightly fluctuated along the operational time, mean ratio values calculated at different operational times are given in Fig. 3B. The contribution of washed-off cations to the overall Ca+Mg+K+Na concentration was generally very large for all biochars. Once Ca+Mg+K+Na concentrations were corrected, a significant relative contribution of cationic exchange to Sm sorption was observed for all tested biochars. CM and PC presented the highest cationic exchange contribution among biochars (78 and 87%, respectively), whereas the contribution was lower for SB and CE materials (25–40%). These values followed the sequence of relative CEC occupancy (see ΣM_{exch}/CEC ratios in Table 1), thus confirming the relevant role of the cationic exchange mechanism in biochars. These results were also in agreement with the good correlation between b and CEC parameters, as previously observed in batch sorption experiments. In addition, other relevant mechanisms may play a significant role in Sm sorption by biochars, such as electrostatic interactions, in agreement with the fact that biochar surfaces were negatively charged (Section 3.1), or inner-sphere surface complexation with oxygen-containing groups, which agrees with lanthanide sorption in biochars reported in literature (Kołodyńska et al., 2018). These functional groups (e.g., carboxylic and carbonyl groups) were confirmed to be present in all biochars, as shown in their FT-IR spectra (Fig. S6 in Supplementary Material), in which C–O and C═O stretching bands, and O–H bending band were observed. These regions of the spectra may be attributed to residual lignin contents in biochars (Horikawa et al., 2019). FT-IR spectra of materials after Sm sorption did not present significant bands' shifts attributable to sorption mechanisms, hence they are not presented here.

Unlike biochars, CF and GAC exhibited a much lower contribution of the washed-off cations to the overall Ca+Mg+K+Na concentrations, which led to significant contributions of the cationic exchange process (72 and 43%, respectively). However, the systematic differences between Sm and Ca+Mg+K+Na exchanged concentrations observed for GAC material indicated an additional, relevant sorption mechanism. Thus, cation exchange played an important role in the sorption process in CF, especially, but also in GAC material, which agreed with their high CEC values and high relative CEC occupancies. Finally, NGAC presented extremely low Ca+Mg+K+Na concentrations during all the experiment and the Sm concentration profile differed to that of the Ca+Mg+K+Na exchanged concentrations, thus indicating the cationic exchange did not play a role in Sm sorption in this material (1% of contribution, see Fig. 3B). This pattern agreed with its low CEC occupancy (around 8%). No characteristic bands of oxygen-containing functional groups were observed in the FT-IR spectra of GAC and NGAC (Fig. S7A), hence discarding surface complexation sorption mechanism. Therefore, the great sorption exhibited by NGAC must have been caused by an alternative mechanism, such as cation-π interactions attributable to its C/O and then high aromaticity, as previously reported (Bandara et al., 2020), which could also be present in GAC. Apart from the scarcity of bands observed, the spectra of Sm-loaded activated charcoals did not register significant bands' shifts attributable to sorption mechanisms.

3.5. Critical comparison of sorption parameters derived from batch and continuous-flow experiments

Maximum sorption capacities derived from continuous-flow experiments ($q_{exp,max}$) and batch sorption tests (b parameter from the Langmuir fitting) were critically compared to finally assess whether the results derived from the two experimental approaches were comparable. Sorption capacities from both sorption methods, expressed in the same units, and the derived correlation can be found in Fig. S7 in Supplementary Material.

The correlation equation between the maximum sorption capacities calculated from batch and continuous-flow experiments had a high regression coefficient ($R^2 = 0.98$), along with a slope and an intercept that did not statistically differ from one and zero, respectively. Thus, batch experiments exhibited sorption capacities matching with the ones obtained experimentally in continuous-flow for the seven materials tested, hence validating both methods as viable ways to quantify at laboratory level the maximum Sm sorption capacity of target sorbent materials. This correlation confirms that differences between the values obtained by the two methods were much lower than differences among materials, confirming the ability of both methods to screen the sorption capacities of candidate materials. Therefore, the choice between the two methods should be based on other criteria rather than on the quantification of the sorption capacities. If information about the sorption process dynamics and sorption progression in time is to be obtained, continuous-flow sorption experiments will be a suitable choice, whereas batch sorption experiments could be more appropriate when testing a high number of materials in a short period of time to obtain information about not only the quantity of sorption sites but also on their quality regarding target contaminant concentration, based on the quantification of the K_d parameter.

4. Conclusions

Batch and continuous-flow sorption experiments permitted to satisfactorily evaluate Sm sorption capacities of tested untreated biochars and carbon-rich materials. The two complementary experimental approaches could be used to determine maximum sorption capacities and screen the viability of candidate materials to be used as sorbents. Batch tests also permitted to identify the materials with highest Sm sorption affinity sites (K_d), whereas sorption percentages exhibited by biochars and coal fines revealed that they could be entirely viable choices to remove Sm from contaminated waters, even without applying any activation treatment to enhance their sorption capacities. Regarding continuous-flow experiments, the non-ideal breakthrough curves obtained made it difficult that Thomas and Yan models could perfectly fit the experimental results, although dynamics of the mechanisms governing sorption could be observed. Cationic exchange was observed to be a relevant mechanism in Sm sorption for all biochars and some carbon-rich materials (CF and GAC), along with other secondary sorption mechanisms proposed, such as surface complexation (for biochars) or cation-π interactions (GAC and NGAC). In this context, results confirm that untreated biochars and coal fines could be satisfactorily applied as a more sustainable and lower cost alternative to commercial activated charcoals to remove Sm, and probably other LN, from contaminated waters at concentrations of environmental concern.

CRediT author statement

Joan Serra-Ventura: Conceptualization, Investigation, Validation, Formal analysis, Writing – Original Draft, Writing – Review & Editing. **Miquel Vidal:** Conceptualization, Investigation, Validation, Writing – Review & Editing, Supervision, Project administration, Funding acquisition. **Anna Rigol:** Conceptualization, Investigation, Validation, Writing – Review & Editing, Supervision, Project administration, Funding acquisition.

Declaration of competing interest

The authors declare that they have no known competing financial interests or personal relationships that could have appeared to influence the work reported in this paper.

Acknowledgements

This work was supported by the Ministerio de Ciencia e Innovación de España (CTM2017-87107-R), the Generalitat de Catalunya (2017

SGR 907) and the RadoNorm Project (funded by Euratom research and training programme 2019-2020 under grant agreement No. 900009). Joan Serra-Ventura acknowledges the fellowship contract from the RadoNorm Project. Authors would like to thank Manel Domínguez for the performance of preliminary experiments.

Appendix A. Supplementary data

Supplementary data to this article can be found online at https://doi.org/10.1016/j.chemosphere.2021.132138.

References

Adeel, M., Yinn, J., Zain, M., Rizwan, M., Nawab, A., Ahmad, M.A., Sha, M., Yi, H., Jilani, G., Javed, R., Horton, R., Rui, Y., Tsang, D.C.W., Xing, B., 2019. Cryptic footprints of rare earth elements on natural resources and living organisms. Environ. Int. 127, 785–800. https://doi.org/10.1016/j.envint.2019.03.022.

Ahmad, M., Rajapaksha, A.U., Lim, J.E., Zhang, M., Bolan, N., Mohan, D., Vithanage, M., Lee, S.S., Ok, Y.S., 2014. Biochar as a sorbent for contaminant management in soil and water: a review. Chemosphere 99, 19–33. https://doi.org/10.1016/j.chemosphere.2013.10.071.

Araneda, C., Basualto, C., Sapag, J., Tapia, C., Cotorás, D., Valenzuela, F., 2011. Uptake of copper (II) ions from acidic aqueous solutions using a continuous column packed with microcapsules containing a β-hydroxyoximic compound. Chem. Eng. Res. Des. 89, 2761–2769. https://doi.org/10.1016/j.cherd.2011.05.008.

Armstrong, C.R., Wood, S.A., 2012. Effect of fulvic acid on neodymium uptake by goethite. J. Colloid Interface Sci. 387, 228–233. https://doi.org/10.1016/j.jcis.2012.07.060.

Bandara, T., Xu, J., Potter, I.D., Franks, A., Chathurika, J.B.A.J., Tang, C., 2020. Mechanisms for the removal of Cd(II) and Cu(II) from aqueous solution and mine water by biochars derived from agricultural wastes. Chemosphere 254, 126745. https://doi.org/10.1016/j.chemosphere.2020.126745.

Boehm, A.B., Bell, C.D., Fitzgerald, N.J.M., Gallo, E., Higgins, C.P., Hogue, T.S., Luthy, R.G., Portmann, A.C., Ulrich, A., Wolfand, J.M., 2020. Biochar-augmented biofilters to improve pollutant removal from stormwater - can they improve receiving water quality? Environ. Sci. Water Res. Technol. 1–18. https://doi.org/10.1039/D0EW00027B.

Ding, W., Dong, X., Ime, I.M., Gao, B., Ma, L.Q., 2014. Pyrolytic temperatures impact lead sorption mechanisms by bagasse biochars. Chemosphere 105, 68–74. https://doi.org/10.1016/j.chemosphere.2013.12.042.

Doumer, M.E., Arízaga, G.G.C., Da Silva, D.A., Yamamoto, C.I., Novotny, E.H., Santos, J.M., Dos Santos, L.O., Wisniewski, A., De Andrade, J.B., Mangrich, A.S., 2015. Slow pyrolysis of different Brazilian waste biomasses as sources of soil conditioners and energy, and for environmental protection. J. Anal. Appl. Pyrolysis 113, 434–443. https://doi.org/10.1016/j.jaap.2015.03.006.

Frišták, V., Micháleková-Richveisová, B., Víglašová, E., Ďuriška, L., Galamboš, M., Moreno-Jimenéz, E., Pipíška, M., Soja, G., 2017. Sorption separation of Eu and as from single-component systems by Fe-modified biochar: kinetic and equilibrium study. J. Iran. Chem. Soc. 14, 521–530. https://doi.org/10.1007/s13738-016-1000-1.

Fu, F., Wang, Q., 2011. Removal of heavy metal ions from wastewaters: a review. J. Environ. Manag. 92, 407–418. https://doi.org/10.1016/j.jenvman.2010.11.011.

Goonan, T.G., 2011. Rare Earth Elements — End Use and Recyclability Scientific Investigations Report 2011 – 5094. U.S. Geol. Surv.

Hadjittofi, L., Charalambous, S., Pashalidis, I., 2016. Removal of trivalent samarium from aqueous solutions by activated biochar derived from cactus fibres. J. Rare Earths 34, 99–104. https://doi.org/10.1016/S1002-0721(14)60584-6.

He, J., Lü, C.W., Xue, H.X., Liang, Y., Bai, S., Sun, Y., Shen, L.L., Mi, N., Fan, Q.Y., 2010. Species and distribution of rare earth elements in the Baotou section of the Yellow River in China. Environ. Geochem. Health 32, 45–58. https://doi.org/10.1007/s10653-009-9264-3.

Horikawa, Y., Hirano, S., Mihashi, A., Kobayashi, Y., Zhai, S., Sugiyama, J., 2019. Prediction of lignin contents from infrared spectroscopy: chemical digestion and lignin/biomass ratios of cryptomeria japonica. Appl. Biochem. Biotechnol. 188, 1066–1076. https://doi.org/10.1007/s12010-019-02965-8.

Iannicelli-Zubiani, E.M., Gallo Stampino, P., Cristiani, C., Dotelli, G., 2018. Enhanced lanthanum adsorption by amine modified activated carbon. Chem. Eng. J. 341, 75–82. https://doi.org/10.1016/j.cej.2018.01.154.

International Biochar Initiative, 2018. URL. https://biochar-international.org/. (Accessed 13 February 2020).

Jinxia, L.I., Mei, H., Xiuqin, Y.I.N., Jiliang, L.I.U., 2010. Effects of the accumulation of the rare earth elements on soil macrofauna community. J. Rare Earths 28, 957–964. https://doi.org/10.1016/S1002-0721(09)60233-7.

Jowitt, S.M., Werner, T.T., Weng, Z., Mudd, G.M., 2018. Recycling of the rare earth elements. Curr. Opin. Green Sustain. Chem. 13, 1–7. https://doi.org/10.1016/j.cogsc.2018.02.008.

Kołodyńska, D., Bąk, J., Majdańska, M., Fila, D., 2018. Sorption of lanthanide ions on biochar composites. J. Rare Earths 36, 1212–1220. https://doi.org/10.1016/j.jre.2018.03.027.

Kulaksiz, S., Bau, M., 2013. Anthropogenic dissolved and colloid/nanoparticle-bound samarium, lanthanum and gadolinium in the Rhine River and the impending destruction of the natural rare earth element distribution in rivers. Earth Planet Sci. Lett. 362, 43–50. https://doi.org/10.1016/j.epsl.2012.11.033.

Kurniawan, T.A., Chan, G.Y.S., Lo, W.H., Babel, S., 2006. Physico-chemical treatment techniques for wastewater laden with heavy metals. Chem. Eng. J. 118, 83–98. https://doi.org/10.1016/j.cej.2006.01.015.

Kütahyali, C., Şert, S., Çetinkaya, B., Inan, S., Eral, M., 2010. Factors affecting lanthanum and cerium biosorption on Pinus brutia leaf powder. Separ. Sci. Technol. 45, 1456–1462. https://doi.org/10.1080/01496391003674266.

Li, H., Dong, X., da Silva, E.B., de Oliveira, L.M., Chen, Y., Ma, L.Q., 2017. Mechanisms of metal sorption by biochars: biochar characteristics and modifications. Chemosphere 178, 466–478. https://doi.org/10.1016/j.chemosphere.2017.03.072.

Liatsou, I., Pashalidis, I., Oezaslan, M., Dosche, C., 2017. Surface characterization of oxidized biochar fibers derived from Luffa Cylindrica and lanthanide binding. J. Environ. Chem. Eng. 5, 4069–4074. https://doi.org/10.1016/j.jece.2017.07.040.

Mahdi, Z., Yu, Q.J., El Hanandeh, A., 2018. Removal of lead(II) from aqueous solution using date seed-derived biochar: batch and column studies. Appl. Water Sci. 8, 1–13. https://doi.org/10.1007/s13201-018-0829-0.

Manyà, J.J., 2019. Advanced Carbon Materials from Biomass: an Overview 164. https://doi.org/10.5281/zenodo.3233733.

Mao, L., Mo, D., Li, M., 2011. The rare earth element compositions of sediments from the loess tableland in the Liyang Plain , southern China : implications for provenance and weathering intensity. Environ. Earth Sci. 62, 1609–1617. https://doi.org/10.1007/s12665-010-0644-x.

Möller, P., Knappe, A., Dulski, P., 2014. Seasonal variations of rare earths and yttrium distribution in the lowland Havel River, Germany, by agricultural fertilization and effluents of sewage treatment plants. Appl. Geochem. 41, 62–72. https://doi.org/10.1016/j.apgeochem.2013.11.011.

Otero, N., Vitòria, L., Soler, A., Canals, A., 2005. Fertiliser characterisation: major, trace and rare earth elements. Appl. Geochem. 20, 1473–1488. https://doi.org/10.1016/j.apgeochem.2005.04.002.

Qiu, Y., Cheng, H., Xu, C., Sheng, G.D., 2008. Surface characteristics of crop-residue-derived black carbon and lead(II) adsorption. Water Res. 42, 567–574. https://doi.org/10.1016/j.watres.2007.07.051.

Rogan, N., Dolenec, T., Sera, T., Dolenec, M., Vrhovnik, P., 2012. Geochemical characteristics of rare earth elements (REEs) in the paddy soil and rice (Oryza sativa L.) system of Kočani Field, Republic of Macedonia. Geoderma 184, 1–11. https://doi.org/10.1016/j.geoderma.2012.03.009.

Ronsse, F., van Hecke, S., Dickinson, D., Prins, W., 2013. Production and characterization of slow pyrolysis biochar: influence of feedstock type and pyrolysis conditions. GCB Bioenergy 5, 104–115. https://doi.org/10.1111/gcbb.12018.

Smith, Y.R., Bhattacharyya, D., Willhard, T., Misra, M., 2016. Adsorption of aqueous rare earth elements using carbon black derived from recycled tires. Chem. Eng. J. 296, 102–111. https://doi.org/10.1016/j.cej.2016.03.082.

Suliman, W., Harsh, J.B., Abu-Lail, N.I., Fortuna, A.M., Dallmeyer, I., Garcia-Perez, M., 2016. Influence of feedstock source and pyrolysis temperature on biochar bulk and surface properties. Biomass Bioenergy 84, 37–48. https://doi.org/10.1016/j.biombioe.2015.11.010.

Tagliaferro, A., Rosso, C., Giorcelli, M., 2020. Biochar: Emerging Applications. IOP Publishing. https://doi.org/10.1088/978-0-7503-2660-5.

Tan, X., Liu, Y., Zeng, G., Wang, X., Hu, X., Gu, Y., Yang, Z., 2015. Application of biochar for the removal of pollutants from aqueous solutions. Chemosphere 125, 70–85. https://doi.org/10.1016/j.chemosphere.2014.12.058.

Thomas, H.C., 1948. Chromatography: a problem in kinetics. Ann. N. Y. Acad. Sci. 49, 161–182.

Torab-Mostaedi, M., Asadollahzadeh, M., Hemmati, A., Khosravi, A., 2015. Biosorption of lanthanum and cerium from aqueous solutions by grapefruit peel: equilibrium, kinetic and thermodynamic studies. Res. Chem. Intermed. 41, 559–573. https://doi.org/10.1007/s11164-013-1210-4.

Xu, N., Ni, J., Sun, W., Borthwick, A.G.L., 2007. Role of dissolved organic carbon in the cosorption of copper and phthalate esters onto Yellow River sediments. Chemosphere 69, 1419–1427. https://doi.org/10.1016/j.chemosphere.2007.04.070.

Xu, Z., Cai, J.G., Pan, B.C., 2013. Mathematically modeling fixed-bed adsorption in aqueous systems. J. Zhejiang Univ. - Sci. 14, 155–176. https://doi.org/10.1631/jzus.A1300029.

Yan, G., Viraraghavan, T., Chen, M., 2001. A new model for heavy metal removal in a biosorption column. Adsorpt. Sci. Technol. 19, 25–43. https://doi.org/10.1260/0263617011493953.

Zhou, B., Li, Z., Chen, C., 2017. Global potential of rare earth resources and rare earth demand from clean technologies. Minerals 7. https://doi.org/10.3390/min7110203.

Zhuang, M., Zhao, J., Li, S., Liu, D., Wang, K., Xiao, P., Yu, L., Jiang, Y., Song, J., Zhou, J., Wang, L., Chu, Z., 2017. Concentrations and health risk assessment of rare earth elements in vegetables from mining area in Shandong, China. Chemosphere 168, 578–582. https://doi.org/10.1016/j.chemosphere.2016.11.023.